INSTITUTE OF PHYSICS PUBLISHING SEMICONDUCTOR SCIENCE AND TECHNOLOGY
Semicond. Sci. Technol. **16** (2001) 345–352 www.iop.org/Journals/ss PII: S0268-1242(01)18376-8

Raman microspectroscopy analysis of pressure-induced metallization in scratching of silicon

Yury Gogotsi[1], Guohui Zhou[2], Sang-Song Ku[2] and Sabri Cetinkunt[2]

[1] Department of Materials Engineering, Drexel University, Philadelphia, PA 19104, USA
[2] Department of Mechanical Engineering, 842 W Taylor Street, University of Illinois at Chicago, Chicago, IL 60607, USA

Received 28 October 2000, accepted for publication 27 February 2001

Abstract
A single-point diamond turning machine was used to make grooves on (111) p-type single-crystal silicon wafers at room temperature. Scratch tests have been performed with both sharp (Vickers and conical) diamond tools, and a spherical (Rockwell) diamond tool. Our results showed that material removal mechanisms differed between these tools. Pressure-induced metallization of Si allows the ductile regime mechanical micromachining of wafer surfaces. Raman microspectroscopy and electron microscopy were used to determine the machining parameters that do not introduce cracking or other types of damage. The surface of the groove, after machining, was covered by a mixture of metastable, high-pressure silicon phases and amorphous silicon. Further, these phases can be transformed into cubic silicon by annealing. The maximum depth of cut in the ductile regime has been determined for the given scratch test conditions and tools. The developed technique can be used to machine Ge, GaAs and other semiconductors. Applications drawing from this research are many. For example, channels for microfluidic devices can be engraved with a channel cross-section that is determined by the shape of the tool, which allows patterns that cannot be produced using etching. There are no limitations on the channel length or direction, and the channel width can vary from potentially a few nanometres to several micrometres.

(Some figures in this article are in colour only in the electronic version; see www.iop.org)

1. Introduction

There is considerable interest focused on the machining of silicon in order to increase the flatness and quality of silicon wafers, and to produce complex-shaped silicon structures for micro-electro-mechanical system (MEMS) applications. Single-point diamond turning was first developed for the production of optical components using nonferrous metals such as aluminum and copper [1, 2]. This technology was later applied to brittle materials such as silicon and germanium [3–5]. Compared to ductile metals [2], the mechanisms of material removal in ductile machining of brittle materials are poorly understood.

During the process of machining, extremely high hydrostatic and deviatoric stresses can be produced, which can induce phase transformation of the work material. In previous studies, the possible mechanisms of brittle to ductile transition during the machining of silicon and germanium were discussed [3, 4], but phase transformations were rarely considered [5]. Our recent work [6] demonstrated that phase transformations occur in a variety of silicon machining operations including slicing, dicing and grinding. We utilized Raman microspectroscopy as a quick and powerful method to characterize phase transformations and measure residual stresses [7–10].

Ultraprecision machining, and specifically nanometric machining, aims at producing high-quality surfaces in terms of surface finish, accuracy and integrity. Many factors, such as tool edge geometry, tool–workpiece interactions, depth of cut, feed rate and control accuracy, affect the quality of the finished

 © 2001 IOP Publishing Ltd Printed in the UK

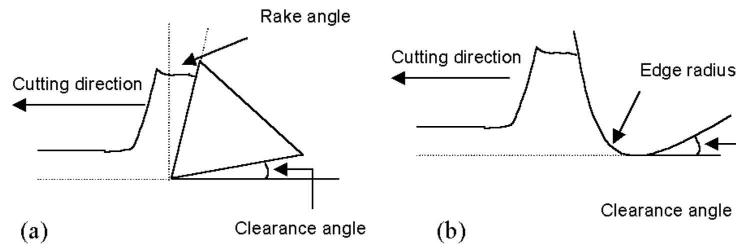

Figure 1. Schematic diagrams showing (*a*) conventional cutting with large γ and (*b*) nanometric cutting with small γ, where $\gamma = \text{(depth of cut)}/\text{(edge radius)}$.

Table 1. Comparison between three tools used in this paper.

	Conical tool	Pyramidal tool (Vickers indenter)	Spherical tool (Rockwell indenter)
Category	Sharp	Sharp	Blunt
Included angle	90°	136°	120° above the sphere
Rake angle	−45°	−68°	Variable, from −90° to about −60°
Material removal	Yes	Yes	No
Densification	Yes	Yes	Yes
Si phases	Si-III, Si-XII, a-Si, Si-IV	Si-III, Si-XII, a-Si, Si-IV	Si-III, Si-XII, a-Si
Maximum stress	Near the edge	Near the edge	In the middle

surface. Both experimental studies and computer simulations of nanoscale machining of semiconductors have been done. Elliptical vibration cutting was investigated [11] in order to reduce the chip thickness and cutting force. The role of rake angle in grinding was studied [12], and it was shown that a more negative rake angle was better for ductile cutting, although the work materials used in that study were limited to metals. Computer simulations have been widely used to aid in the study of semiconductor machining [13–15] and in analysing the structures of machined surfaces [16]. The limitation in the computer simulations is that the simulated depth of cut can reach only several nanometres. This is much smaller than the real depth of cut, which ranges from about several hundred nanometres to tens of micrometres. The problems in current computer simulations occur because the pressure-induced metallization cannot be simulated with the depth of cut above several nanometres. Therefore, experimental determination of the transformation depth is required.

In conventional cutting, the edge radius of the tool is negligible in magnitude when compared to the depth of cut. In nanometric cutting, this is generally not the case due to small depths of cut and a minimum possible edge radius of 20–70 nm (figure 1). However, for a worn or dull single-crystal diamond tool, the tip becomes rounded and the radius increases.

It is established that silicon undergoes a sequence of phase transformations under static contact loading [7,9]. Amorphous silicon has been found [17] during microcutting tests, and a semiconductor–metal (brittle-to-ductile) phase transformation in low-load scratching of silicon was proposed [5] based on TEM and SEM studies. However, no direct evidence of pressure-induced metallization was provided in those papers.

The purpose of the current research is to investigate the stress and phase distributions, material removal mechanisms, and the mechanism of the brittle-to-ductile transition in scratches on silicon.

2. Experimental setup and test procedure

A single-point diamond turning (SPDT) machine was developed and used in this paper. It consists of a high-precision air-bearing spindle and an X–Y stage. The guideways of the machine tool axis are double V type, which gives extremely repeatable straight motion in the X–Y plane of table movement. This type of guideway, however, also has a high level of friction due to the metal surface contact and sliding. Friction characterization tests on a similar machine at the National Institute of Standards and Technology (NIST) determined the static friction threshold to be approximately 5.6 N m [18]. Position measurement is obtained with the optical encoders attached to the motors and a laser interferometer system for direct table position measurements. The equivalent linear resolution of the motor encoder with the effective gear reduction is approximately 2.11 nm. The laser interferometer resolution is 2.5 nm. These two measurement systems are used for a dual-feedback arrangement to ensure the stability in the presence of backlash and to obtain accurate table positioning.

Lightly doped (111) p-type single-crystal silicon wafers of 150 mm diameter were cut into pieces with 10 mm by 10 mm dimensions. Scratches were made using conical, pyramidal and spherical diamond tools (table 1). The tool was mounted on the SPDT machine during experiments. The conical tool, with a 90° included angle, was a low-cost commercial diamond scriber with a tip that was not perfectly sharp. It was supposed to simulate an abrasive grain of irregular shape. The second tool was a calibrated Vickers indenter from Wilson (division of Instron, US) with a 136° included angle and tip radius of less than 100 nm. Both the faces and edges of the pyramidal tool can be used to make scratches, and in this paper, the face of the tool was used. The third tool was a standard conical Rockwell indenter from Wilson with a spherical tip of about 200 μm radius. Among these tools, the spherical tool has the largest

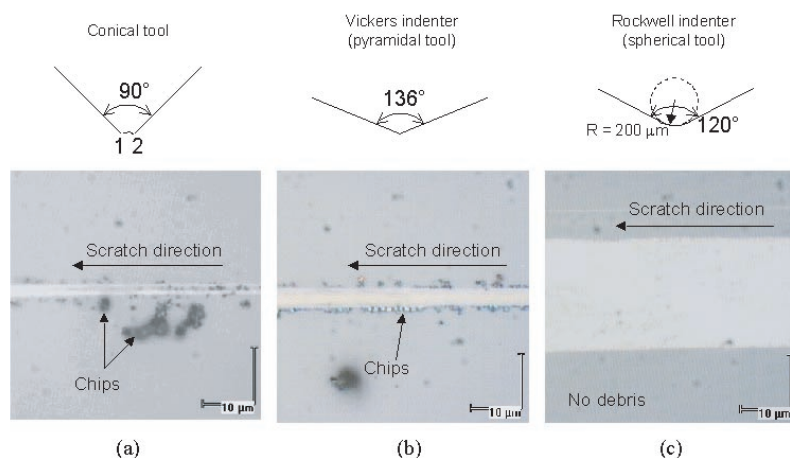

Figure 2. Optical micrographs of scratches showing ductile chips produced using (*a*) a conical tool, (*b*) a pyramidal tool and (*c*) a spherical tool.

tip radius. All the tools have negative rake angles and can be used to simulate ductile-regime machining of silicon. On the macroscale, they are classified as sharp tools with negative rake angles. A pyramid with a 136° included angle would be equivalent to a high negative rake angle of $-68°$. Also, the sphere would be similar to a varying high negative rake angle from close to $-90°$ at the point of contact to whatever the angle subtended by the tool is at the depth of cut line. The scratching speed in our experiments was 10 μm s^{-1}. A gap sensor was used to detect the contact point where the diamond tip touched the surface of the sample. This contact point was treated as the zero depth. Cutting depth was increased gradually until cracks were formed. After scratching, a Raman microspectrometer (Renishaw 2000) was used to acquire Raman spectra in a back-scattering geometry. The point analysis was conducted with the spot size of 1 μm ($\times$100 objective lens). A motorized XYZ stage was used for mapping phase composition and strain with 0.5 μm step size. Although two-dimensional maps were plotted, autofocusing was used to ensure pin-point accuracy during confocal mapping. The maps were produced using GRAMS-32 and Renishaw Wire software, which enables peak fitting with a Lorentzian or Gaussian function as described in [6, 8]. Peak positions determined using peak fitting were plotted to create strain maps with the spectral resolution better than 0.1 cm^{-1}. The excitation wavelength of 514.5 nm of an argon ion laser was used. Field-emission scanning electron microscopy (JEOL 6320F), atomic force microscopy (Digital Instruments) and optical profilometry (Ade Phase Shift) were used to analyse the morphology of scratches, pile-ups and chips.

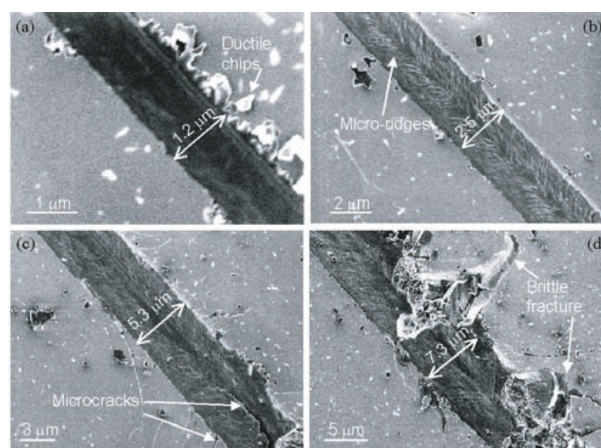

Figure 3. SEM micrographs of scratches produced by a sharp pyramidal tool. Silicon exhibits (*a*), (*b*) ductility on a microscale and (*c*), (*d*) brittle fracture at the depth of cut above the critical value.

3. Results

3.1. Effect of tool geometry

The tool geometry and optical micrographs of selected scratches are shown in figure 2. The scratch in figure 2(*a*) was made by the conical tool with an imperfect tip. At the starting point of the scratch, two grooves are obtained (figure 2(*a*)), but as the tool is dragged while increasing the depth, these two grooves merge into one. The scratch made by the conical tool is quite similar to that made by the pyramidal tool (figure 2(*b*)), but obviously different from that produced by the spherical tool (figure 2(*c*)). A large amount of debris was found alongside the scratches made by the conical and pyramidal tools. However, for the scratch made by the spherical tool, no debris or chips were observed. This suggests different material removal mechanisms by the sharp (conical and pyramidal) and blunt (spherical) tools.

3.2. Scratch topography

SEM images provide information on the topography of the scratch produced using the pyramidal tool. Figure 3(*a*) shows the ductile debris. The ‘celery stalk’ micro-ridges can be seen in the groove in figures 3(*b*)–(*d*). These micro-ridges denoted material plastic flow following the tip during scratching. This process was accompanied by tremendous deformation. When the deformation exceeded the limit or the tensile stress exceeded the strength of the wafer, microcracks (marked in figure 3(*c*)) formed in order to release the elastic energy. Cracking was first observed when the groove width exceeded about 5 μm. In figure 3(*d*), the observed brittle

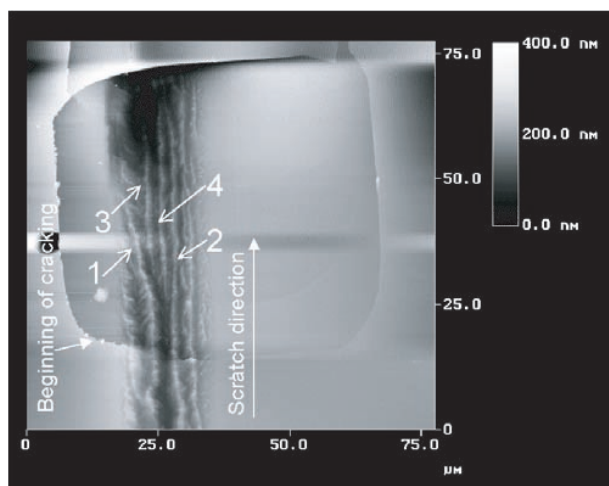

Figure 4. AFM image of the scratch produced by the spherical tool. Micro-ridges 3 and 4 were formed between ridges 1 and 2. The orientation and number of ridges change along the scratch.

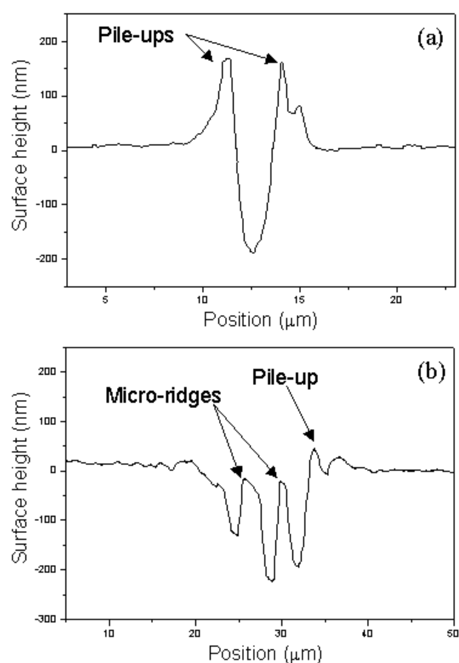

Figure 5. Surface profiles of scratches obtained using an optical profilometer. A high ratio of height of pile-up to depth proves the significant ductility of silicon under the tool. (*a*) Pyramidal tool, depth/width = 0.05, height of pile-up/depth = 0.89, (*b*) spherical tool, depth/width = 0.016, height of pile-up/depth = 0.24.

material removal produced large chips. If the depth of cut increases further, the wafer cracks. The critical depth for microcracking was measured to be 270 nm for the pyramidal tool and 250 nm for the spherical tool.

It is important to compare the topography of the scratch made by the pyramidal and spherical tools. Figure 4 is an AFM image of the scratch made by the spherical tool. There are three to five micro-ridges inside the scratch. The phenomenon did not result from the irregularity of the tip, because the direction of the ridges changed along the scratch. In figure 4, ridges 1 and 2 deviated at a certain position, and two new ridges 3 and 4 formed. If the tip shape caused this topography, the

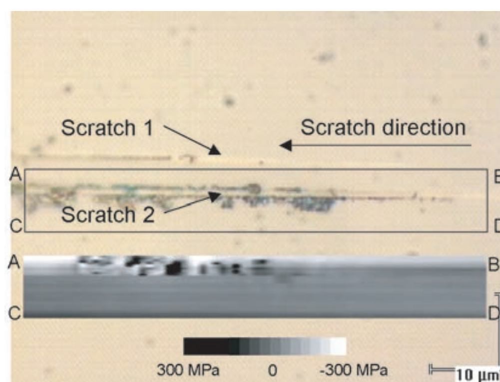

Figure 6. Optical micrograph of a scratch produced by the conical tool and an overlaid Raman stress map of the framed area. Higher compressive stresses exist in the area between the scratches because two scratches are very close and material in that area is squeezed between the tips during scratching.

pattern should not have changed along the whole scratch. In figure 3(*b*), the pattern of ridges was almost the same along the whole scratch, with small ridges starting from the edge and ending in the middle of the groove. Plastic flow may only partially account for the patterns shown in figures 3 and 4, as will be discussed later.

In the crack-free region of scratches, the ratio of depth to width of the scratch made by the spherical tool is much smaller than that of the pyramidal tool. This ratio is 0.015 for the spherical tool and 0.05 for the pyramidal tool (figure 5), the ratio for the spherical tool being smaller because the spherical tip is much blunter than the pyramidal one. Pile-ups, which were observed along the scratches, can significantly affect the groove profile. For example, the height of the pile-up was 136 nm for the pyramid scratch with the depth of 152 nm, and 36 nm for the sphere scratch with the depth of 243 nm. The significant pile-up comparable with the groove depth in the case with the pyramidal tool shows the higher ductility of silicon on a microscale.

3.3. Stress analysis

The residual stresses near the scratch were calculated from the up- or downshift of the LO + 2TO Raman band of silicon in the cubic diamond phase (Si-I) assuming a biaxial stress state [19]. The stress map and image of a scratch made by the conical tool are shown in figure 6. At the beginning of the scratch, the corresponding residual stresses in the material are low because of the small depth of cut. The cutting falls into the ductile regime with minimal damage and no cracks. The highest residual stress was measured along the edge AB. The area between the two scratches was squeezed from both sides and high compressive stresses formed during scratching. It is necessary to note that Raman spectroscopy analysis measures an average value of compressive/tensile stress and the stress sensitivity coefficient of 3.2 cm^{-1} GPa^{-1} used was determined for the biaxial stress state [10]. The complex stress state and material damage around scratches may result in an increase in the full width at half maximum (FWHM) of the Si-I peak and, sometimes, in peak splitting [24]. However, since the peak position and integral intensity determined after deconvolution and fitting were plotted, peak broadening did not have a

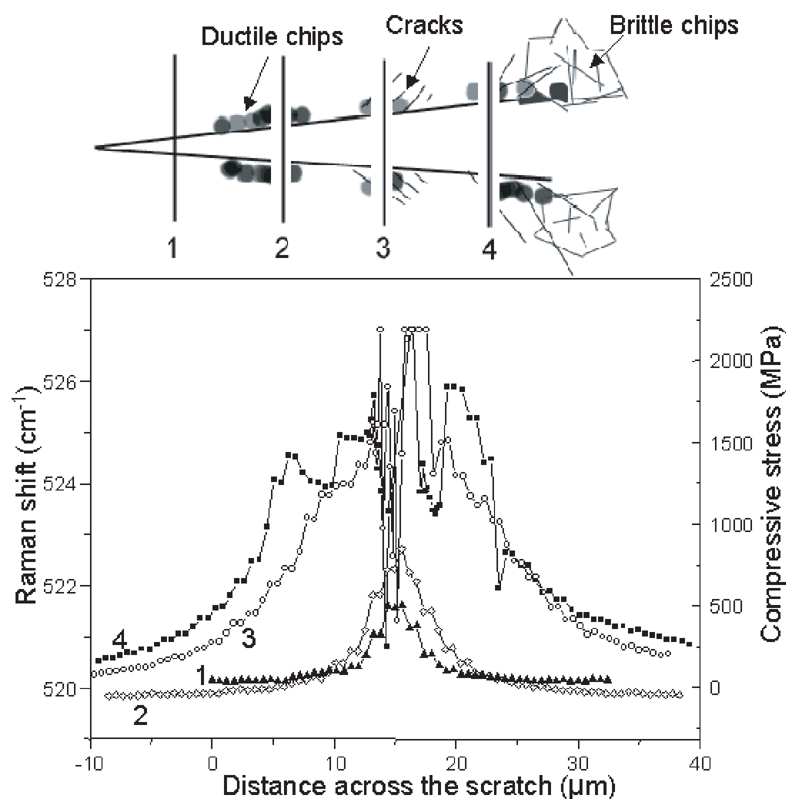

Figure 7. Raman line scans across the scratch showing that the residual stress increases with the depth of cut. Scan 1 is in the ductile region with no debris, scan 2 is in the ductile region with ductile chips and debris, scan 3 is in the cracking region and scan 4 is in the brittle chipping region. Strong variations of stresses close to the centre of the groove in scans 3 and 4 are due to cracking and local stress relaxation.

significant effect on the accuracy of stress maps. In figure 6, low residual stresses (almost invisible in the inset in figure 6) are present outside the scratches and relatively high residual stresses are present between the scratches. Low stress outside the scratch produced with a small depth of cut shows the possibility of ductile regime machining of silicon with minimal residual stresses.

The residual stresses increased with the depth of cut (figure 7). When the contact area between the tool and the silicon wafer increases, pressure under the tool becomes insufficient to drive the phase transformation and the deformation cannot be accommodated for in a ductile manner. At that moment, the fracture of the silicon wafer starts and the created cracks cause the stresses to reduce. Figure 7 shows the stress distribution along the scratch made by the pyramidal tool in which four different final conditions were chosen for residual stress measurements. Scan 1 was taken from the ductile region, when the depth of cut was minimal. Scan 2 was taken from the region where debris formed, scan 3 was taken from the region where there was cracking and scan 4 was taken for the region in which there was brittle chipping. As can be seen in figure 7, the residual stresses increase with the depth of cut. Once cracks form, the local strains around the cracks relax, leading to strong stress variation in scans 3 and 4. In figure 8, an optical micrograph of the cracked region is presented together with the stress distribution along the AD line. In the cracking zone, the average measured residual stress is much lower than that in the crack free zone because the elastic strain is released by cracking.

3.4. Phase analysis

Regardless of the tool shape, similar phase composition is revealed after the test by Raman spectroscopy. Figure 9 shows the typical spectra acquired in the grooves made by different tools. The phases that frequently appear in the grooves are Si-III (*bc*8, body-centred cubic structure [20]), Si-XII (*r*8, the rhombohedral distortion of *bc*8 [7]) and amorphous silicon (a-Si [10]). For certain conditions, Si-IV (*hd*, hexagonal diamond structure [20]) was sometimes found in the groove (figure 9(*a*)). Usually Si-III and Si-XII are present in the vicinity of the edge of the groove or in the pile-up region, as the result of squeezing metallic Si phase out of the centre of the groove. In contrast, smaller amounts of these phases were found in the middle of the groove, where the material had been scraped away by the tool tip. Amorphous and nanocrystalline Si were found in shallow grooves (shown in figure 6), before other phases appeared. Si-IV was found to form earlier than other polymorphs of silicon. However, it is worth noting that the assignment of the peak at 500–510 cm^{-1} to the *hd* phase [20, 21] is still arguable, because nano- and cryptocrystalline silicon may produce a band located in this wavenumber range [22, 23]. Similar ‘double-peak’ features in the Raman spectra taken from certain areas of the groove in silicon and from some of the debris along the groove flanks were interpreted as arising from the bulk Si-I and from the small domains of crystalline Si formed within the parent amorphous phase by a recrystallization process [17]. Raman shifts as large as 7 cm^{-1}, corresponding to residual stresses of 2.2 GPa, were observed (figure 9(*c*)). Under contact loading, silicon undergoes a series

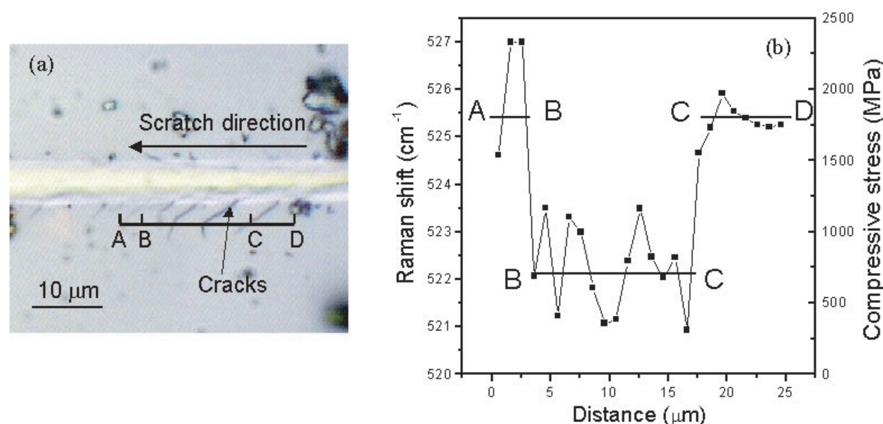

Figure 8. Stress relaxation in the cracking zone. (*a*) Optical micrograph of a scratch produced using a pyramidal tool, (*b*) stress profile along AD line.

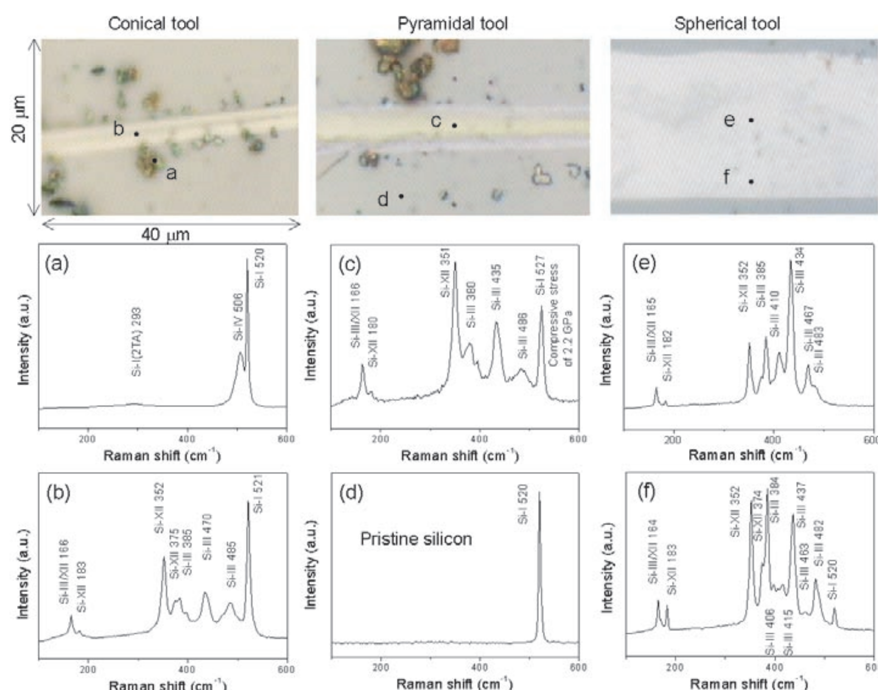

Figure 9. Raman spectra acquired from different areas with a 1 μm spot size. Spectra show the presence of Si-III, Si-XII, Si-IV and amorphous silicon in the groove. Positions of major Raman bands are marked.

of phase transformations [24]. If the hydrostatic pressure reaches 10–13 GPa, metallic phase Si-II (β-Sn) forms from the semiconducting Si-I. Metallic Si-II is not stable below ~4 GPa [25] on unloading and transforms to other phases depending on pressure release conditions. Amorphous silicon is obtained upon fast unloading and a mixture of Si-XII and Si-III can form during relatively slow unloading [7, 9]. In our scratch experiments, the scratching speed was constant. At a small depth of cut, the residual stresses are relatively small. This leads to a faster stress decrease than at a large depth, when significant residual stresses and the constraint of surrounding material results in a slow reverse transformation. Therefore, amorphous silicon is formed at a small depth of cut, while Si-III, Si-XII and Si-IV are formed at a larger depth of cut.

It is established that Si-III and Si-XII can only be formed via β-tin silicon (Si-II) [24]. There are strong indications that amorphous silicon observed after contact loading is also formed from the metallic Si-II phase in the unloading stage [24]. Thus, the observation of metastable phases (Si-III and Si-XII) and amorphous material in the scratches made in silicon wafers with tools of different geometry supports the notion of pressure-induced metallization during scratching. Typical phase distributions in the groove are shown in figure 10. The groove was covered by a mixture of metastable phases, mainly Si-III, Si-XII and a-Si. Due to the highly localized stresses underneath the tool, metallic Si-II was formed and consequently transformed to a-Si and other phases, such as Si-III and Si-XII, behind the tool. However, the amount of polymorphs in the groove produced by the pyramidal tool was much less compared to the groove formed using the spherical tool, because most of the transformed material was removed from the scratch by the movement of the sharp tool.

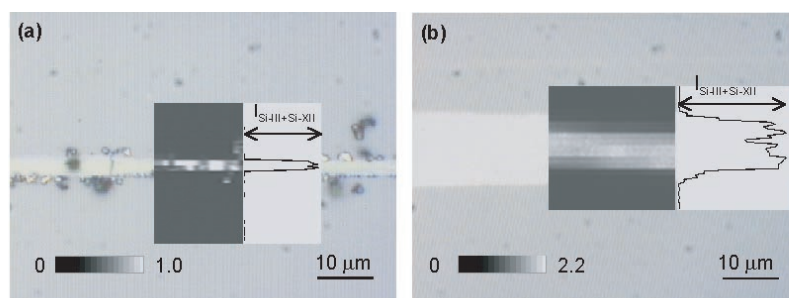

Figure 10. Optical micrographs with overlaid phase distributions and line scans across the scratches. The grooves made by the pyramidal and spherical tools were covered by a mixture of Si-III and Si-XII. The line scans show the relative intensity of Si-III + Si-XII. (*a*) $I_{\text{Si-III+Si-XII}}/I_{\text{Si-I}}$ in the scratch made by the pyramidal tool, (*b*) $I_{\text{Si-III+Si-XII}}/I_{\text{Si-I}}$ in the scratch made by the spherical tool.

The reverse phase transformation from metallic silicon to metastable phases behind the tip, which is accompanied by $>10\%$ volume increase, can be responsible for a complex morphology within the groove shown in figure 4.

4. Discussion

The results of the analysis of scratches made by three different tools are summarized in table 1. The Raman spectra from the grooves and chips demonstrated the phase transformation and formation of metastable phases including a-Si, Si-III, Si-XII and Si-IV. The chips produced during ductile regime machining were also examined [26] and found to be partially amorphous. Pressure-induced metallization occurred under a variety of machining conditions such as slicing, dicing, grinding and lapping, and the same metastable phases as those in the scratch tests were found [6]. This shows that the material removal mechanism in scratching is similar to that in machining. Moreover, machining operations including cutting and turning produce extremely high hydrostatic and deviatoric stresses under the work-tool. Therefore, we can substitute the complicated machining with a relatively simple scratching in search for operation conditions for ductile-regime cutting.

For silicon, if we control the depth of cut, ductile machining can be achieved with a sharp tool that has a high negative rake angle. For brittle materials with phase transformations, such as Si, we suggest the material removal mechanism to be the transformation to the metallic phase and ductile removal of that phase. Semiconductor-to-metal transition plays a key role in the ductile machining of semiconductors. The micro-ridges in figures 4 and 3(*b*) and pile-ups in figure 5 demonstrate plastic flow during scratching, which would be impossible in the hard and brittle semiconductor state of silicon. It is known from plasticity theory that the yield strength of a material is determined by the deviatoric stress state, while the magnitude of the hydrostatic stress determines the extent of plastic deformation prior to fracture. Many brittle materials are capable of ductile behavior, but only under high hydrostatic pressure [27]. Thus, a high value of the hydrostatic pressure is the required driving force for phase transformation and a prerequisite for plastic flow of the ductile metallic phase of silicon formed under pressure. All three tools used in the current research provide sufficient pressures to enable the transformation of Si-I to metallic Si-II and plastic deformation of the material beneath the tool. However, it is necessary to remember that only ductile metallic Si can be deformed to the extent observed.

The mechanisms of material removal for sharp tools (conical or pyramidal) and blunt tools (spherical) have been found to be different. Ductile chips are produced using a sharp tool and no debris is produced using a blunt tool. In the latter case, silicon underneath the tip is highly compressed and transformed to denser polymorphs. The formation of the groove can be accounted for by the volume difference between Si-I and high-pressure polymorphs, as well as in the formation of pile-ups. As an example of practical application, tools with spherical tips can be used to make shallow nanoscale channels in silicon with depth smaller than 200 nm without any debris. When the metallization occurs on the Si surface, the metallic layer is <1 μm deep and the remaining transformed layer is only about 100 nm in thickness [28]. The penetration depth of the 514.5 nm green laser radiation into the bulk Si is about 340 nm [29]. Consequently, the presence of transformed phases within the bulk of the $\sim$340 nm thick layer is detected by a Raman spectrometer. Brittle fracture leaves damage to the underlying layers as deep as 5–10 μm, which is due to multiple cracks. For ductile cutting, a substantial amount of time and chemicals would be saved by eliminating etching or decreasing the depth of etching that is currently used to remove the damaged layers from machined surfaces.

The case of grinding and polishing using a diamond wheel or abrasive slurry is much more complex than simple scratching, but the mechanism of material removal is essentially the same. The numerous particles on the wheel or in the abrasive act as many small tips, producing different contact pressures and creating different depths of cut due to their respective shape and size. Thus, metallization, plastic deformation and brittle fracture may occur simultaneously. The machining conditions and abrasive particle shapes and sizes will determine which of the above processes dominate. Practically, we need to suppress microfracture and enhance metallization to achieve the ductile regime. This leads to a tremendous opportunity to predict the experimental conditions for ductile regime machining of brittle materials from scratch tests.

Ductile regime machining with sharp tools may be used as an alternative for marking (engraving) semiconductor wafers, which is currently done using lasers. It can also produce deep grooves in Si wafers that are required for MEMS or microfluidic devices, which are finding increasing application in analytical and biomedical systems. Conventional methods

for fabricating microfluidic devices have centred on etching channels in glass and silicon [30, 31]. By applying the ductile cutting techniques discussed in this paper, we can employ a sharp tool to produce complicated microfluidic channels without introducing brittle fracture. This method is not dependent on the crystal orientation, and channel shapes other than that permitted by the selective etchant and crystal structure can be produced. Slight etching may be used after this method is employed to remove the metastable phases and decrease residual stresses.

5. Conclusions

(1) Raman spectroscopy shows the presence of metastable silicon phases in scratches produced on silicon wafers using three different diamond tools. They provide the evidence of the formation of metallic Si, which is beneficial for ductile-regime machining. Metallic Si-II transforms to Si-XII, Si-III and Si-IV or amorphous silicon behind the moving tool.
(2) The mechanism of material removal during scratching, using a sharp tool, involves ductile removal of the metallic phase to a critical depth of cut when microfracture starts. The critical depth of cut depends on the tool shape. Microfracture can be suppressed by controlling the depth of cut.
(3) The residual stresses increase with the depth of cut. The highest residual stress is shown to exist in the vicinity of the pile-up.
(4) No material is removed during scratching of silicon using a blunt tool with a spherical tip. The volume change, or densification, during phase transformation and plastic flow of metallic silicon accounts for the formation of the groove.
(5) Semiconductor-to-metal transition (pressure-induced metallization) has been shown to play a key role in the process of ductile regime machining of brittle materials. A combination of scratch tests and Raman spectroscopy analysis can be used to optimize and monitor ductile regime machining of semiconductors.

Acknowledgments

The authors are thankful to Mr V Domnich for assistance with SEM analysis and helpful discussions, Mr N Kalashnikov for help with AFM analysis and Mr T Juliano for proofreading the paper (all with the University of Illinois at Chicago), Dr A Kovalchenko, Argonne National Laboratory, for help with optical profilometry and Dr F Kirscht, Mitsubishi Silicon America, for Si wafers. This paper was supported by a grant from the US National Science Foundation DMI-9813257.

References

[1] Krauskopf B 1984 *Manuf. Eng.* **92** 90
[2] Shaw M C 1984 *Metal Cutting Principles* (Oxford: Oxford University Press)
[3] Blackley W S and Scattergood R O 1994 *J. Eng. Industry* **116** 263
[4] Blake P N and Scattergood R O *Ductile-Regime Turning of Germanium and Silicon* NASA-TM-101231, N89-20322
[5] Morris J C and Callahan D L 1994 *J. Mater. Res.* **9** 2907
[6] Gogotsi Y, Baek C and Kirscht F 1999 *Semicond. Sci. Technol.* **14** 936
[7] Gogotsi Y G, Kailer A and Nickel K G 1997 *Mater. Res. Innovat.* **1** 3
[8] Gogotsi Y G and Gardner M A 2000 *The Americas Microscopy and Analysis*, March 2000 p 11
[9] Kailer A, Gogotsi Y G and Nickel K G 1997 *J. Appl. Phys.* **81** 3057
[10] Lucazeau G and Abello L 1997 *J. Mater. Res.* **12** 2262
[11] Shamoto E and Moriwaki T 1994 *CIRP Ann.* **43** 35
[12] Komanduri R 1971 *Int. J. Mach. Tool Des. Res.* **11** 223
[13] Inamura T, Takezawa N, Kumaki Y and Sata T 1994 *CIRP Ann.* **43**
[14] Isono Y and Tanaka T 1999 *JSME Int. J.* **42** 158
[15] Komanduri R, Chandrasekaran N and Raff L M 1998 *Wear* **219** 84
[16] Shimada S, Ikawa N, Tanaka H and Uchikoshi J 1994 *CIRP Ann.* **43**
[17] Tanikella B V and Somasekhar A H 1996 *Appl. Phys. Lett.* **69** 2870
[18] Larsen G S and Cetinkunt S 1997 *ASME J. Dyn. Syst. Meas. Control* **119** 775
[19] De Wolf I 1996 *Semicond. Sci. Technol.* **11** 139
[20] Kobliska R J and Solin S A 1973 *Phys. Rev.* B **8** 3799
[21] Weill G, Mansot J L, Sagon G, Carlone C and Besson J M 1989 *Semicond. Sci. Technol.* **4** 280
[22] Zhao X S, Ge Y R, Schroeder J and Persans P D 1994 *Appl. Phys. Lett.* **65** 2033
[23] Zi J, Buscher H, Falter C, Ludwig W, Zhang K and Xie X 1996 *Appl. Phys. Lett.* **69** 200
[24] Domnich V and Gogotsi Y 2001 *Handbook of Surfaces and Interfaces* ed H S Nalwa (New York: Academic) vol 2 ch 5 at press
[25] Domnich V, Gogotsi Y and Dub S 2000 *Appl. Phys. Lett.* **76** 2214
[26] Morris J C, Callahan D L, Kulik J, Patten J A and Scattergood R O 1995 *J. Am. Ceram. Soc.* **78** 2015
[27] Bridgman P W 1953 *J. Appl. Phys.* **24** 405
[28] Puttick K E, Whitmore L C, Ycynes C and Gee A E 1996 *Proc. ASPE Spring Topical Meeting on Precision Grinding of Brittle Materials* p 82
[29] Pizani P S, Jasinevicius R, Duduch J G and Porto J V 1999 *J. Mater. Sci. Lett.* **18** 1185
[30] Richter K, Orfert M, Howitz S and Thierbach S 1999 *Surf. Coatings Technol.* **119** 461
[31] Stjernstrom M and Roeraade J 1998 *J. Micromech. Microeng.* **8** 33